RSC Applied Polymers

PAPER

View Article Online
View Journal

Cite this: DOI: 10.1039/d5lp00400d

A thiophene-based and sulfur-enriched highly conjugated hyper-crosslinked polymer for efficient sequestration of iodine from various media

Sk Abdul Wahed, Mustafa Maqbool, Atikur Hassan * and Neeladri Das *

Received 16th December 2025,
Accepted 1st March 2026

DOI: 10.1039/d5lp00400d

rsc.li/rscapplpolym

A thiophene-based hyper-crosslinked polymer (Bi-Thio HCP) was synthesized using commercially available 2,2′-bithiophene as a monomer *via* Friedel–Crafts alkylation reaction. The obtained Bi-Thio HCP exhibits a high surface area, hierarchical porosity, and an abundance of electron-rich binding sites, facilitating efficient and rapid iodine uptake. The Bi-Thio HCP demonstrated a modest iodine capture capabilities, with an adsorption capacity of 1.96 g g^{-1} in the vapor phase at 350 K and a maximum uptake capacity of 1.66 g g^{-1} for triiodide (I_3^-) in aqueous phase at 298 K. The distribution coefficient (K_d) values greater than 10^5 mL g^{-1} associated with I_3^- capture indicate the high affinity of an adsorbent material towards the adsorbate. The trapped iodine can be readily released by simple heating at an elevated temperature or by soaking in an alcoholic solvent (such as methanol and ethanol) at room temperature. The Bi-Thio HCP can be recycled for at least five cycles without any significant decrease in removal efficiency, enabling its use in sustainable applications. In this study, the adsorption capacities and mechanisms of iodine adsorption by Bi-Thio HCP material were examined using Density Functional Theory (DFT) computations. Overall, the Bi-Thio HCP is a highly competitive adsorbent for iodine sequestration, thanks to its ease of synthesis from readily available monomers and scalable reaction conditions.

1. Introduction

The use of nuclear energy to generate electricity is gaining popularity worldwide.[1] According to the "World Nuclear Association", more than four hundred nuclear power reactors are operational worldwide, and these contribute to approximately 13% of the global electricity generation.[2,3] Since electricity generated from nuclear energy has a significantly lower carbon footprint than the thermal power plants,[4,5] the contribution of nuclear energy to global electricity production is likely to experience substantial growth in the next few decades.[6] However, on the flipside, electricity production from nuclear power plants is associated with the generation of radioactive waste.[7] Disposal of nuclear waste (having a high level of radioactivity) safely and effectively remains a significant challenge. During the processing of the spent nuclear fuel (SNF) with concentrated HNO_3, substantial quantities of the radioisotopes of iodine undergo oxidation to produce volatile molecular iodine, which is released into off-gas streams (OGS).[8,9] In addition, nuclear reactor cooling systems are also known to release radioactive iodine into water bodies, harming aquatic ecosystems and posing significant health hazards.[10] Of the many radionuclides found in nuclear power plant waste, iodine-129 (^{129}I) and iodine-131 (^{131}I) are particularly dangerous. A unique characteristic of iodine-129 is its exceptionally long half-life of approximately 15.7 million years.[11] On the other hand, iodine-131 (^{131}I) has a relatively much shorter half-life of 8.02 days.[12] ^{131}I is used as a nuclear medicine for the treatment of thyroid cancer or other thyroid problems because it emits radiations of significantly higher energies.[13,14] However, upon bioaccumulation of ^{131}I in healthy cells (of the thyroid), it can also cause cancer.

The release of radioactive iodine isotopes into water bodies has far-reaching effects not only on aquatic ecosystems but also on human health. As an example, the human metabolic system has been exposed to radioactive iodine that emerged from the chernobyl nuclear accident,[15,16] leading to a rise in diseases such as thyroid cancer among the human population in those regions.[17] Therefore, it is essential to ensure the selective capture and sequestration of radioactive iodine-containing species from the environment.[18] In the near future, it will also support the safer and sustainable usage of nuclear energy over alternative power generation sources.

The current method for capturing radioactive gases from OGS is wet scrubbing.[19] However, there are some practical drawbacks, including high operating costs, ineffective separation, and the creation of secondary contaminants in the form

Department of Chemistry, Indian Institute of Technology Patna, Patna, Bihar-800106, India. E-mail: atikurhassan@gmail.com, neeladri@iitp.ac.in, neeladri2002@yahoo.co.in

of hazardous, corrosive, and carcinogenic liquid wastes. The challenges associated with "wet scrubbing techniques" can be resolved by the use of solid-state porous adsorbents.[20] In this context, several porous materials have been proposed as potential adsorbents,[21] including metal–organic frameworks (MOFs),[22,23] Ag-exchanged zeolites,[24] graphene-based aerogels,[25] activated carbons,[26] and porous organic polymers (POPs).[26,27] But every material has its own set of advantages and disadvantages. For example, robust and simple-to-make Ag-exchanged zeolites are costly, have a low potential for adsorption, and are not highly recyclable.[28–30] The yield of radioactive AgI precipitate, a secondary pollutant, is another concern. Since the dissolver solution in the SNF facility is highly acidic, MOFs that are unstable at acidic pH are ineffective as adsorbent.[31,32] Compared to these materials, amorphous POPs such as Hyper-cross-linked Polymers (HCPs), Conjugated Microporous Polymers (CMPs), Polymers of Intrinsic Microporosity (PIMs), and Porous Aromatic Frameworks (PAFs) are more appropriate for real-world applications like reversible iodine capture because of their favourable properties, such as good thermal and physicochemical stabilities.[18,33–35]As a result, POPs have recently been developed and synthesized especially for energy storage, gas capture, catalysis, drug delivery, and other various uses.[36–39] In the context of iodine capture, the affinity and the maximum adsorption capacity of the POPs for the gaseous iodine molecules may be significantly raised by incorporation of electron-rich heteroatom groups [such as nitrogen (N), oxygen (O), sulfur (S)] within the polymeric framework.[40–43] Hyper-cross-linked polymers (HCPs) are a unique class of POPs that were first identified by Davankov and Tsyurupa in 1969.[44] To date, a wide variety of HCPs have been synthesized that are decorated with various structural motifs and heteroatoms in their polymeric network. While there are many reports of HCPs with N or O as the heteroatoms, there are only a handful of HCPs that contain softer Lewis basic S atoms incorporated in the polymeric backbone.[45–47]

In this work, we design a thiophene-based hyper-cross-linked polymer (HCP) using commercially available yet inexpensive 2,2′-bithiophene as a monomer *via* the facile Friedel–Crafts alkylation reaction. The obtained thiophene-based adsorbent (Bi-Thio HCP) has an ample number of electron-rich sulphur heteroatoms. After complete characterization using various techniques, we were curious to explore the performance of this S-rich HCP as an improved adsorbent for iodine species, including gaseous I_2. The iodine adsorption capability of Bi-Thio HCP was measured to be 1.96 wt%. The mechanism of interaction between the trapped iodine and the thiophene motifs is also examined in this work. Experimental data obtained using various techniques were used to investigate the chemical and physical interactions between iodine molecules and the thiophene motif of Bi-Thio HCP. Additionally, using DFT calculations, valuable insights related to the corresponding structure–property interactions are presented. The ensuing sections provide a detailed description of the experimental results.

2. Experimental section

2.1 Materials

2,2′-Bithiophene, formaldehyde dimethyl acetal (FDA), and anhydrous ferric chloride ($FeCl_3$) was purchased from Sigma-Aldrich. 1,2-Dichloroethane, methanol, acetone, cyclohexane, THF, and molecular iodine were purchased from commercial sources such as Spectrochem, Finar, or CDH. All reagents and solvents used in this work were of analytical grade and used without further purification.

2.2 Synthesis of Bi-Thio HCP

Bi-Thio HCP was synthesized *via* the well-known Friedel–Crafts alkylation reaction using 2,2′-bithiophene as the monomer (Scheme 1). Concisely, 2,2′-bithiophene (166.26 mg, 1.0 mmol) was added to a 50 mL round-bottom flask under a nitrogen (N_2) atmosphere and dissolved in 25 mL of 1,2-dichloroethane (DCE). 5 mL of formaldehyde dimethylacetal (FDA) and anhydrous ferric chloride (811 mg, 5 mmol) were added in sequence. The reaction mixture was refluxed at 85 °C for 24 h under an N_2 atmosphere. Following the completion of the reaction, the obtained precipitate was filtered and thoroughly washed with methanol, tetrahydrofuran (THF), and acetone to remove $FeCl_3$ from the polymer matrix. Furthermore, the washed product was suspended in methanol for 24 hours to remove any soluble impurities using the Soxhlet extraction technique. The desired product, Bi-Thio HCP, was obtained as a dark brown powder by drying the purified material in a vacuum oven at 100 °C for 12 hours.

2.3 Iodine capture experiment

2.3.1 Static iodine uptake by Bi-Thio HCP. The non-radioactive ^{127}I was used throughout the entire experiment as a surrogate for radioactive iodine since all isotopes of iodine are known to have similar chemical properties. In a typical iodine adsorption experiment, 20 mg of Bi-Thio HCP was placed in a pre-weighed open glass vial, which was kept inside a larger vessel containing crystals of molecular iodine at the bottom. To promote iodine sublimation and produce a steady atmosphere of iodine vapour, the closed system was kept at 77 °C. Iodine uptake was monitored by recording the mass change of the polymer at regular time intervals. The amount

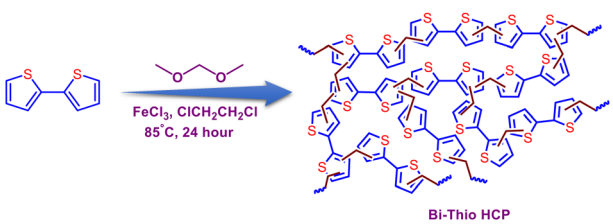

Scheme 1 Synthesis of Bi-Thio HCP *via* Friedel–Craft alkylation reaction.

of iodine uptake of the Bi-Thio HCP was calculated by using eqn (1)

$$\text{Iodine uptake}(g\,g^{-1}) = \frac{M_2 - M_1}{M_1} \quad (1)$$

Herein, M_1 is the weight of the Bi-Thio HCP before iodine uptake, and M_2 is the weight of the Bi-Thio HCP after iodine uptake.

To investigate the kinetics of the iodine capture by Bi-Thio HCP and obtain mechanistic insights, the iodine adsorption data were fitted with the following linear equations corresponding to the pseudo-first-order (eqn (2)) and pseudo-second-order (eqn (3)) rates.

$$\ln(Q_e - Q_t) = \ln Q_e - k_1 t \quad (2)$$

$$\frac{t}{Q_t} = \frac{1}{k_2 Q_e{}^2} + \frac{1}{Q_e} t \quad (3)$$

Here, Q_e and Q_t are the iodine uptake capacity of Bi-Thio HCP at equilibrium (e), and at a particular time (t) interval, respectively, while k_1 (h^{-1}) and k_2 (g mg^{-1} h^{-1}) are rate constants of the pseudofirst-order and second-order reaction, respectively.

2.3.2 Iodide uptake by Bi-Thio HCP from aqueous medium. An I_3^- solution was prepared by dissolving specified quantities of I_2 and potassium iodide (KI) in water. To measure the kinetics associated with I_3^- removal from water by Bi-Thio HCP, we first determined the absorbance of a freshly prepared aqueous I_3^- solution (50 ppm). Subsequently, a measured dose of adsorbent (Bi-Thio HCP, 50 mg) was added to a 50 mL aqueous I_3^- solution (50 ppm). UV-visible spectra were recorded at regular time intervals by drawing 2 mL of aliquots. Based on the UV-visible data, the percentage of iodide removed from the water was estimated using eqn (4), and the capture capacity was calculated using eqn (5).

$$\%\,\text{removal} = \frac{C_0 - C_t}{C_0} \times 100 \quad (4)$$

$$\text{Uptake capacity}\,(Q_t) = (C_0 - C_t) \times \frac{V}{M} \quad (5)$$

Here, C_0 (ppm) and C_t (ppm) represent the initial concentration and concentrations of I_3^- at a particular time (t), respectively. Q_t represents the capture capacity (g g^{-1}) at time (t). V represents the volume of the I_3^- solution, and M is the weight of the Bi-Thio HCP polymer used in the adsorption experiment.

In adsorption isotherm studies, I_3^- solution concentrations ranged from 50 to 2000 ppm. In these studies, 2.5 mg of adsorbent (Bi-Thio HCP) was soaked in 5 ml of the respective I_3^- solution for 12 hours. Later, 2 mL of the supernatant was removed for UV-vis measurement. To gain insight into the sorption mechanism, the I_3^- sorption isotherm data were fitted with the equations corresponding to the Freundlich isotherm model (eqn (6)) and the Langmuir isotherm model (eqn (7)).

$$\ln Q_e = \ln K_F + \left(\frac{1}{n}\right) \ln C_e \quad (6)$$

$$\frac{C_e}{Q_e} = \frac{1}{K_L Q_m} + \frac{C_e}{Q_m} \quad (7)$$

Here, Q_e (mg g^{-1}) is the quantity of I_3^- adsorbed at equilibrium, and C_e (ppm) is the corresponding equilibrium concentration; Q_m (mg g^{-1}) is the maximum quantity of I_3^- adsorbed to form a monolayer on the surface of the adsorbent. K_L (L mg^{-1}) is the Langmuir constant, and K_F is the Freundlich constant.

2.3.3 Iodine adsorption by Bi-Thio HCP from *n*-hexane solution. The kinetics of the removal of I_2 from *n*-hexane were examined. First, we recorded the absorbance of a freshly prepared solution (100 ppm) of I_2 in *n*-hexane. Subsequently, 50 mg of Bi-Thio HCP polymer was added to 50 mL of I_2 in *n*-hexane solution, and the mixture was stirred at room temperature. At different time intervals, 2 mL of aliquots were drawn from the mixture to record the corresponding UV-visible spectra. Based on the UV-visible data, the percentage of iodine removed from the *n*-hexane solution was estimated using eqn (4). To calculate the maximum uptake capacity of iodine from *n*-hexane solution, 5 mL solutions of various concentrations were exposed to 2.5 mg of Bi-Thio HCP. After 12 hours of continuous stirring, 2 mL of the supernatant was removed for UV-vis measurement. Eqn (5) was used to determine the maximum uptake capacity.

2.3.4 Selectivity study of I_3^- by Bi-Thio HCP. The I_3^- removal efficiency of Bi-Thio HCP was also examined in the presence of anions (such as Br^-, NO_3^-, PO_4^{3-} and SO_4^{2-}) that are commonly found in wastewater. In these experiments, a molar ratio of 1 : 1 was maintained between I_3^- and another anion to assess the performance of the adsorbent (Bi-Thio HCP) in the presence of competing ions. The adsorbent (2.5 mg) was suspended in 5 mL of the prepared 50 ppm solution, and the mixture was stirred for 3 hours. Subsequently, 2 mL of the supernatant was collected, and UV-vis spectra were recorded to measure the residual concentration of I_3^- anions in the solution.

2.3.5 Recyclability and reusability of the iodine-loaded Bi-Thio HCP. In the desorption experiments, a measured quantity of the iodine-captured polymer (I_2@Bi-Thio HCP) was placed in 15 mL of colorless methanol solution and stirred for 6 hours. During that time, the solution color changed to brown. The colored solution was decanted and refilled with fresh methanol every hour until a clear solution was achieved. The polymer was filtered, cleaned with copious quantities of water and alcohol, air-dried, and then reused in a subsequent cycle as an adsorbent.

2.3.6 Density functional theory (DFT) study. The density functional theory (DFT) methodology was used with the B3LYP function to optimize the interaction between a single repeating unit of Bi-Thio HCP and I_2, I_3^- adsorbed structure of Bi-Thio

HCP using a basis set of 6-311G(d,p) or SDD. The interaction energy was calculated using the following equation and the relative energies of Bi-Thio HCP, I_2@Bi-Thio HCP, and I_3^-@Bi-Thio HCP.

$$\Delta E = E_{(\text{Bi-Thio HCP+iodine species})} - E_{(\text{Bi-Thio HCP})} - E_{(\text{iodine species})}$$

Here, $E_{(\text{Bi-Thio HCP+iodine species})}$ represents the optimized energy after adsorption of iodine species, $E_{(\text{Bi-Thio HCP})}$ denotes optimized energy of Bi-Thio HCP alone, and $E_{(\text{iodine species})}$ corresponds to the optimized energy of various iodine species such as I_2, I_3^-.

3. Results and discussion

3.1 Characterization of Bi-Thio HCP

POPs have emerged as a popular class of functional materials due to their unique characteristics, such as facile synthesis with high yields, adjustable porous structures, hierarchical porosity with high surface areas, and ease of incorporating various building blocks and functional groups. Using appropriately functionalized monomers, it might be feasible to develop porous materials with numerous Lewis basic sites that can interact with the electron-deficient iodine species. With this objective, the Bi-Thio HCP was synthesized (Scheme 1) *via* the well-known Friedel–Crafts alkylation reaction using 2,2′-bithiophene as the monomer (detailed synthesis procedures are provided in the Experimental section). To obtain a pristine polymer free from by-products and unreacted monomers, the resulting crude product was washed with several solvents, including methanol, THF, and acetone. Fourier transform infrared (FTIR) spectrum of Bi-Thio HCP was recorded to identify the distinct functional groups present. In the FT-IR spectrum of the polymer, the appearance of new bands at ~2871 and ~2965 cm^{-1} corresponds to the symmetric and antisymmetric stretching vibrations of the methylene group, which are absent in the monomer spectrum and thus confirm the successful formation of the polymer network (Fig. 1a).[48] Furthermore, several bands appeared between 1620 cm^{-1} and 1060 cm^{-1}, which correspond to the stretching and bending of C=C and C=S bonds present in the thiophene units.[49] In the solid-state ^{13}C CP-MAS NMR spectrum of Bi-Thio HCP, peaks appearing in between 120 ppm and 140 ppm were attributed to substituted and non-substituted aromatic carbon atoms. Additionally, the resonance peak at 22 ppm corresponds to the methylene carbons in the Bi-Thio HCP network that crosslink one monomer unit with another (Fig. 1b).[50] The powder X-ray diffraction (PXRD) pattern of Bi-Thio HCP revealed broad peak suggesting its amorphous nature (Fig. 1c). To investigate the thermal stability of Bi-Thio HCP, a sample was subjected to thermogravimetric analysis (TGA) by heating it between 30 and 800 °C under nitrogen environment (Fig. 1d). The TGA thermogram of Bi-Thio HCP shows the polymeric material has good thermal stability with the thermal degradation tempera-

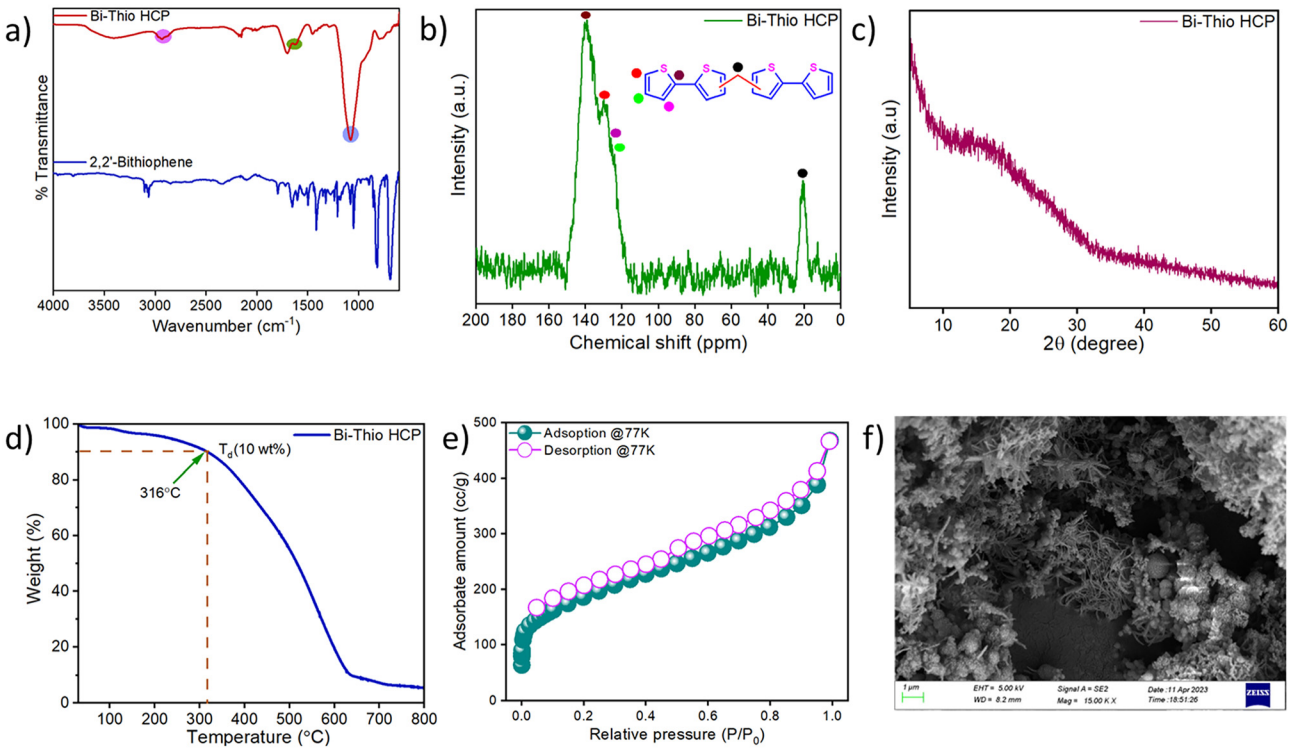

Fig. 1 (a) FT-IR spectra of 2,2′-Bithiophene (monomer) and Bi-Thio HCP (polymer). (b) Solid state ^{13}C-NMR (CP/MAS) of Bi-Thio HCP. (c) PXRD pattern of Bi-Thio HCP (d) Thermogravimetric Analysis (TGA) of Bi-Thio HCP. (e) N_2 sorption isotherm of Bi-Thio HCP at 77 K. (f) FESEM image of Bi-Thio HCP.

ture (T_d = 10% weight loss) at around 316 °C. The nitrogen sorption isotherm was recorded at 77 K to gather information related to the pore structure and surface area. Before surface area analysis, the Bi-Thio HCP sample was activated by heating under vacuum at 120 °C for 12 hours. In the N_2 sorption isotherm curves (Fig. 1e), the Bi-Thio HCP demonstrated rapid N_2 gas uptake at low relative pressures (P/P_0 < 0.01), suggesting the presence of a significant number of micropores in the polymeric network. The BET surface area of Bi-Thio HCP was calculated from the low-temperature nitrogen sorption isotherm and was found to be 664.10 $m^2\ g^{-1}$ (Fig. S1). Using nonlocal density functional theory (NL-DFT), the pore size distribution of Bi-Thio HCP was obtained, and it was concluded that the material was microporous with an average pore size of around 1.61 nm (Fig. S2). Due to the inherent porosity in Bi-Thio HCP, the CO_2 sorption capacity of Bi-Thio HCP was measured at two temperatures and atmospheric pressure. The CO_2 uptake capacities of Bi-Thio HCP were found to be 83 mg g^{-1} at 273 K (Fig. S3) and 42 mg g^{-1} at 298 K (Fig. S4). These data suggest the effective CO_2 adsorption capabilities of the Bi-Thio HCP polymer, and its performance is comparable to that of several other previously reported polymers under identical conditions. The Field Emission Scanning Electron Microscopy (FESEM) data were used to gain insights into the morphology of Bi-Thio HCP. The micrograph showed a highly porous and rough surface texture with an interconnected network of aggregated particles (Fig. 1f). The presence of carbon (C) and sulfur (S) elements in the network of Bi-Thio HCP was confirmed by energy dispersive X-ray spectroscopy (EDS) mapping analysis (Fig. S5). CHNS elemental analysis was performed to confirm the composition of the synthesized Bi-Thio HCP. CHNS elemental analysis showed that Bi-Thio HCP consists of 66.06% carbon, 3.26% hydrogen and 22.86% sulfur, respectively (Fig. S6). The presence of ample heteroatoms and high surface area (>650 $m^2\ g^{-1}$) due to the microporous nature of Bi-Thio HCP motivated us to explore the polymeric material's suitability as an adsorbent for iodine sequestration applications.

3.2 Iodine capture study

To perform iodine vapor adsorption studies, a pre-weighed sample of Bi-Thio HCP was placed inside a small glass vial, which was subsequently kept in a larger container (containing a crystal of molecular iodine) that was capped securely and put in an oven preheated to ~77 °C.[51] Periodically, the inner glass vial was brought out and weighed to measure the quantity of iodine trapped by Bi-Thio HCP. For nearly complete saturation of the adsorbent (Bi-Thio HCP) with the adsorbate (I_2) and to reach the equilibrium conditions, the material has to be exposed to iodine vapors for nearly 48 hours. Upon iodine uptake, a prominent color change was observed in Bi-Thio HCP from dark brown to black (Fig. S7). Upon saturation of Bi-Thio HCP with iodine (I_2@Bi-Thio HCP), as evident from negligible weight increment, the weight of the sample was noted to calculate the maximum iodine uptake capacity using eqn (1). Thus, the iodine uptake capacity of Bi-Thio HCP was found to be 196 wt% (Fig. 2a) using the gravimetric analysis method. The iodine uptake of Bi-Thio HCP is comparable to that of

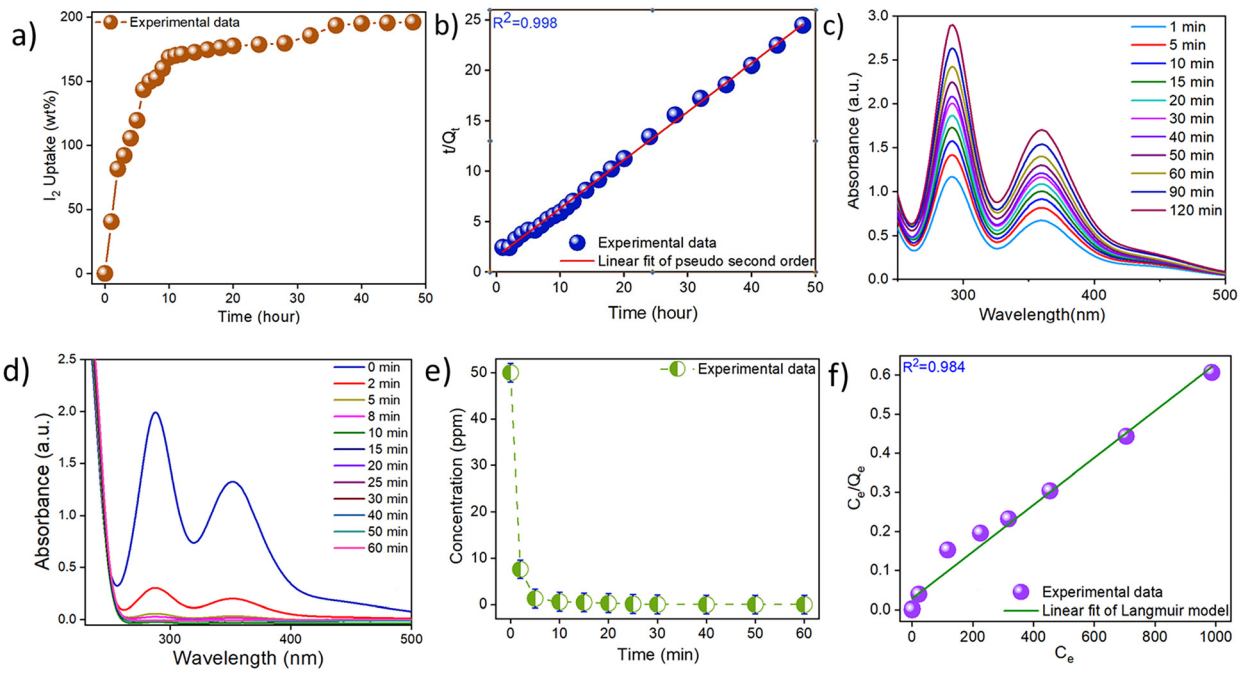

Fig. 2 (a) Gravimetric measurement of I_2 vapor uptake of Bi-Thio HCP at 77 °C. (b) Pseudo-second-order linear fit of iodine capture by Bi-Thio HCP. (c) Release of iodine from I_2@Bi-Thio HCP in methanol. (d) UV-vis spectra of gradual uptake of I_3^- from aqueous solution by Bi-Thio HCP. (e) I_3^- kinetic plot of Bi-Thio HCP. (f) Langmuir isotherm model of Bi-Thio HCP for I_3^-.

several previously reported adsorbents, which are considered high-performing materials (Table S1). The efficiency of Bi-Thio HCP as an adsorbent for iodine in the vapor phase might be due to its aromatic backbone and heteroatom-rich polymer network. Subsequently, the kinetics associated with iodine capture were explored. Experimental data (Fig. S8) fitted well with the pseudo-second-order kinetics rate equation, yielding a correlation coefficient value of 0.998 (Fig. 2b). Iodine recovery from I_2@Bi-Thio HCP was thoroughly investigated by heating the iodine-loaded sample or immersing it in methanol solvent. In this context, a known quantity of I_2@Bi-Thio HCP sample was heated at 125 °C in an open glass vial, and the weight loss was recorded periodically due to the gradual release of the trapped iodine. Approximately 60% of the adsorbed iodine was released in the first hour, and 86% of iodine was released over the following six hours (Fig. S9). Because of the irregular/non-uniform distribution of pore sizes, some iodine molecules remained trapped in the polymeric network. To conduct an iodine desorption experiment under wet conditions and without the application of heat, a sample of I_2@Bi-Thio HCP was immersed in 15 mL of neat methanol placed inside a 20 mL glass vial. Periodically, the UV-Vis spectra of the methanol solution were recorded. The iodine release from I_2@Bi-Thio HCP was monitored for 120 minutes using UV-vis spectroscopy (Fig. 2c). As more iodine was released over time, the solvent's color slowly changed from colorless to light yellow and finally deep brown (Fig. S10). Accordingly, the absorbance of the peaks with maxima at 290 and 358 nm continued to increase, indicating the presence of iodine species in methanol.[52] This confirmed the effective release of iodine species present on the surface or trapped within the pores of Bi-Thio HCP. This further confirmed the presence of iodine on the surface and within the pores of Bi-Thio HCP that was gradually released into the methanol solution. Reusability of the material is a desirable and essential characteristic in any good adsorbent from the perspective of its sustainable use. Experimental data showed that Bi-Thio HCP could efficiently capture iodine (163 wt%) in the fifth cycle, indicating a minor decrease in its performance as an adsorbent (Fig. S11). Thus, Bi-Thio HCP performs effectively as an iodine adsorbent since it can be easily regenerated while rapidly releasing most of the trapped iodine under ambient conditions.

The performance of Bi-Thio HCP as an adsorbent of I_3^- ions was examined by adding 50 mg of Bi-Thio HCP to a 50 mL solution of I_3^- (50 ppm) and using UV-vis spectroscopy to monitor the adsorption kinetics. With the gradual passage of time, monitoring the changes in the absorbance of the peaks centered at 352 and 287 nm provided valuable insights into the gradual adsorption of triiodide from the aqueous medium.[51] The absorbance of these peaks gradually decreased, indicating that Bi-Thio HCP was effective as an adsorbent in removing triiodide from the aqueous solution (Fig. 2d). Almost 90% adsorption of I_3^- ions was trapped within five minutes. More than 99% of triiodide were adsorbed within twenty minutes (Fig. 2e and Fig. S12). The results were fitted using pseudo-first-order (Fig. S13) and pseudo-second-order (Fig. S14) rate equations to gain a better understanding of the kinetics associated with triiodide capture. A high correlation coefficient (0.999) was obtained upon fitting the data to the pseudo-second-order rate equation. Compared to the Freundlich model (Fig. S15), a better fit of the adsorption isotherm data was obtained using the Langmuir model (Fig. 2f), suggesting monolayer adsorption of adsorbate species (I_3^-) on the surface of the adsorbent (Bi-Thio HCP). Using the Langmuir isotherm model, the maximum iodide adsorption capacity of Bi-Thio HCP from water was calculated to be 1663.34 mg g^{-1}. A comparison with previously reported adsorbents of iodide species from aqueous solution suggested that Bi-Thio HCP has superior performance (Table S2). A variety of anions, such as Br^-, NO_3^-, OAc^-, CO_3^{2-}, SO_4^{2-}, and PO_4^{3-}, are commonly found in water samples in nature. Therefore, iodine capture experiments were performed in the presence of other ions to test whether Bi-Thio HCP selectivity traps iodide. Experimental data (Fig. S16) clearly indicated that the adsorption of the iodide remained unaffected in the presence of other competing anions that were present at a 1 : 1 molar ratio in simulated samples of iodine-contaminated wastewater. Thus, capture studies using a binary mixture of anions ratified Bi-Thio HCP's effectiveness in selective uptake of iodide. The distribution coefficient (K_d) is commonly used to assess the affinity of a sorbent toward different sorbates. Adsorbent materials with a K_d value above 10^4 mL g^{-1} are considered promising adsorbents. The K_d value of Bi-Thio HCP for I_3^- removal was determined to be 4.4×10^5 mL g^{-1}.

To measure the efficiency of Bi-Thio HCP as an adsorbent of molecular iodine present in aqueous media, we performed adsorption tests using saturated aqueous iodine solutions (1 mM). In these experiments, 50 mg of Bi-Thio HCP was added to iodine solution (50 mL, 1 mM). The color of the solution changed from yellow to colorless, which the unaided eye could easily perceive. This change was quantified using UV-vis spectral data, which showed a decrease in peak intensity at 461 nm (Fig. 3a).[53] The Bi-Thio HCP was able to remove almost 80% of the iodine from the aqueous solution in 8 minutes and more than 95% of the iodine in 20 minutes, according to the time-dependent UV-vis data (Fig. S17). Overall, the Bi-Thio HCP was able to remove 99% of iodine from an aqueous solution. Both pseudo-first-order (Fig. S18) and pseudo-second-order (Fig. 3b) kinetics models were used to investigate the mechanism of iodine uptake from aqueous solutions. The kinetics data of the iodine removal process fitted well with the pseudo-second-order model ($R^2 > 0.99$). On the other hand, the pseudo-first-order kinetics model showed a lower correlation coefficient ($R^2 = 0.954$). Subsequently, the maximum iodine uptake capacity from water was estimated using iodine solutions with concentrations ranging from 50 to 250 ppm. The adsorption isotherm data showed an excellent fit to the Langmuir isotherm model (Fig. 3c), with a high correlation coefficient ($R^2 = 0.995$), compared to the Freundlich isotherm model (Fig. S19) indicating that the adsorption process follows Langmuir isotherm model. Using the Langmuir isotherm model (Fig. 3c), the maximum adsorption capacity of

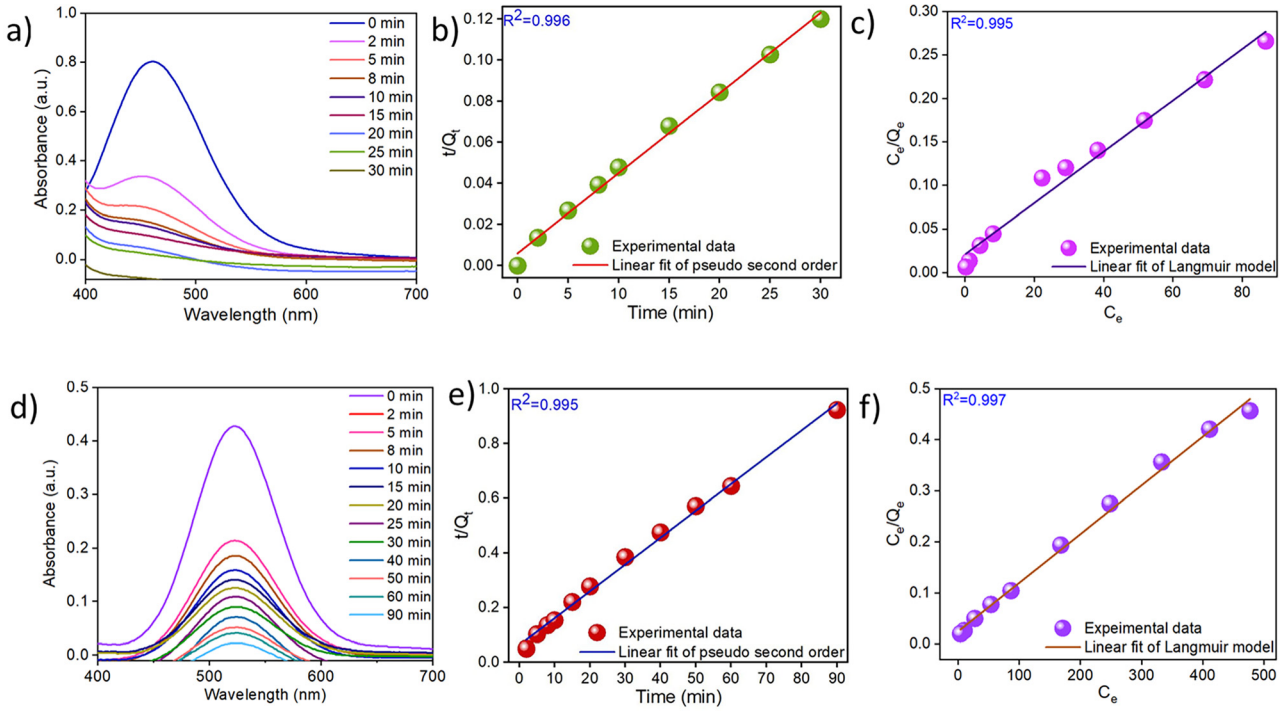

Fig. 3 (a) UV-vis adsorption spectra of I_2 adsorption from aqueous solution by Bi-Thio HCP. (b) Pseudo-second-order linear fit for iodine adsorption from aqueous solution by Bi-Thio HCP. (c) Langmuir isotherm model for iodine adsorption from aqueous solution by Bi-Thio HCP. (d) Time-dependent UV-vis spectra of the gradual uptake of I_2 from *n*-hexane solution by Bi-Thio HCP. (e) Pseudo-second-order linear fit for iodine adsorption from *n*-hexane solution by Bi-Thio HCP. (f) Langmuir isotherm model for iodine adsorption from *n*-hexane solution by Bi-Thio HCP.

iodine from aqueous solutions was calculated to be 348.98 mg g^{-1}. Next, we were interested in assessing the performance of Bi-Thio HCP as an adsorbent to trap iodine dissolved in organic solvents, such as hexanes. A pristine sample of Bi-Thio HCP was added to a purple-colored hexane solution of iodine. The UV-vis spectra of the iodine *n*-hexane solution were recorded at various time intervals to monitor the rate of iodine uptake by Bi-Thio HCP (Fig. 3d). The decrease in the intensity of the absorption maxima of the UV-vis spectra with the gradual progress of time indicated that the Bi-Thio HCP was successful in removing dissolved iodine from its *n*-hexane solution. The UV-vis data showed that over 90% of the dissolved iodine was captured by Bi-Thio HCP within 60 minutes (Fig. S20). The kinetics of iodine capture by Bi-Thio HCP from *n*-hexane solution (Fig. 3e and Fig. S21) were calculated from the spectral data. It was found that the data fitted more precisely with the pseudo-second-order model (correlation coefficient of 0.995) than the pseudo-first-order equation. Additionally, iodine capture experiments were performed using solutions of varying concentration (100 to 1000 ppm) to understand the mechanism of iodine adsorption by Bi-Thio HCP from *n*-hexane solutions (Fig. 3f and Fig. S22). Using the Langmuir model for data fitting (Fig. 3f), the maximal absorption capacity was determined to be 1049.31 mg g^{-1}. The appreciably high iodine absorption capacity of Bi-Thio HCP suggests that several variables, including surface area, pore size, and the presence of an electron-rich heteroatom in the framework, contribute to its performance. Iodine adsorption in the Bi-Thio HCP is primarily driven by donor–acceptor and charge-transfer interactions between sulfur lone pairs in the bithiophene units and iodine species. Molecular iodine (I_2) is destabilized *via* electron donation to the σ* antibonding orbital of the I–I bond, while triiodide (I_3^-) is non-covalently stabilized through electron acceptance at terminal iodine atoms. These interactions, together with chalcogen bonding and π-electron delocalization within the conjugated network, enhance iodine adsorption.

3.3 Post capture characterization

Iodine-loaded Bi-Thio HCP (I_2@Bi-Thio HCP) samples were examined using several analytical techniques, including FT-IR, PXRD, Raman spectroscopy, EPR, and FESEM), to gain a better understanding of the iodine adsorption mechanism. These characterizations provide valuable information regarding the chemical and morphological changes in the Bi-Thio HCP after iodine adsorption, which in turn help understand the adsorption process. The FT-IR spectra of the Bi-Thio HCP before and after iodine capture are compared in Fig. 4a, wherein noticeable changes in the peak positions of interacting functional groups are observed. For example, the bands corresponding to the C=S and C=C stretching vibrations in the pristine polymer (Bi-Thio HCP) shifted after iodine adsorption (I_2@Bi-Thio HCP). The observed spectral shift suggested that the sulfur atoms and the arene rings serve as interaction or

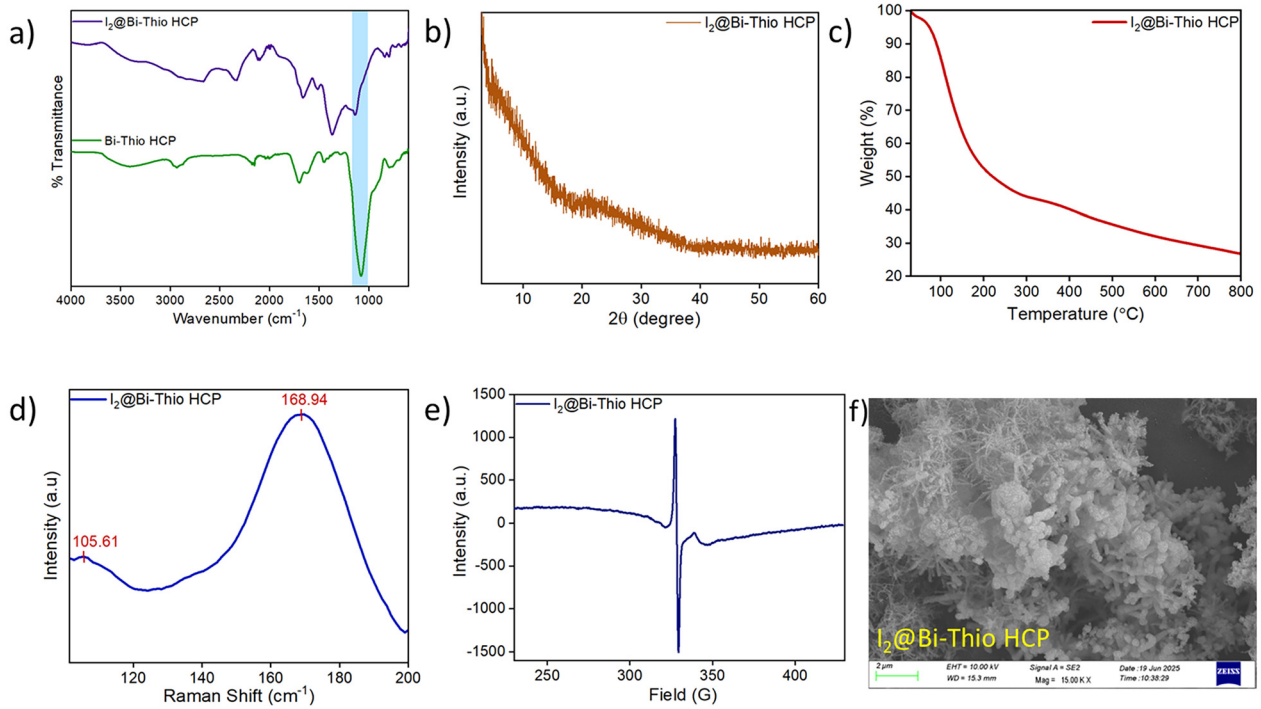

Fig. 4 (a) FT-IR spectra of I_2@Bi-Thio HCP compared with pristine Bi-Thio HCP. (b) PXRD pattern of iodine-loaded Bi-Thio HCP (I_2@Bi-Thio HCP). (c) TGA plot of iodine-loaded Bi-Thio HCP (I_2@Bi-Thio HCP). (d) Raman spectrum of I_2@Bi-Thio HCP. (e) EPR spectrum of I_2@Bi-Thio HCP (f) FESEM image of I_2@Bi-Thio HCP.

binding sites for the molecular iodine. The PXRD pattern of I_2@Bi-Thio HCP showed that the polymer remained amorphous after iodine capture (Fig. 4b) and there were no diffraction peaks corresponding to crystalline iodine. The thermogravimetric analysis (TGA) of I_2@Bi-Thio HCP was performed by heating the sample under a nitrogen atmosphere. The corresponding TGA thermogram revealed a significant weight loss between 80–400 °C due to the progressive release of adsorbed iodine from the I_2@Bi-Thio HCP (Fig. 4c). Raman spectral data were further used to find out the nature of iodine species present in I_2@Bi-Thio HCP. The I_2@Bi-Thio HCP showed two distinct peaks at 105.6 and 168.9 cm^{-1}, which are characteristic of polyiodide anions (Fig. 4d).[54] These peaks represent the "V or L" shaped configurations of I_5^-, suggesting that these polyiodide species were formed on the surface of the Bi-Thio HCP after iodine adsorption.[20,55] The presence of charge transfer interactions in I_2@Bi-Thio HCP was confirmed by EPR analysis.[56] The existence of radical species was evidently revealed by a strong signal in a sample of I_2@Bi-Thio HCP (Fig. 4e). Radicals are generated because of facile electron transfer between iodine and the electron-rich groups in the HCP network of Bi-Thio HCP.[57] While a comparison of the FESEM images of pristine Bi-Thio HCP (Fig. 1f) and I_2@Bi-Thio HCP (Fig. 4f) revealed no noticeable morphological changes, a significant iodine content in the I_2@Bi-Thio HCP sample was further confirmed by the elemental mapping data and EDX analysis, with the latter suggesting a uniform distribution of iodine inside the polymer network (Fig. S23).

3.4 DFT study

To better comprehend the experimental findings, theoretical investigations using DFT were performed utilizing B3LYP hybrid density functional with a 6-311G or SDD basis set (details in section 4 of SI).[58] Initially, DFT computations were performed on the single repeating unit of Bi-Thio HCP to understand the extent of iodine adsorption by aromatic heterocyclic rings containing an S atom. Additionally, RDG (Reduced Density Gradient) and QTAIM (Quantum Theory of Atoms in Molecules) were employed for analysis, as these techniques are frequently used to gain a deeper understanding of molecular structure, chemical bonding and nonbonding interactions, and reactivity. The model of the DFT-optimized structures of Bi-Thio HCP, I_2@Bi-Thio HCP, and I_3^-@Bi-Thio HCP is presented in Fig. S24. The calculated binding energies for I_2@Bi-Thio HCP and I_3^-@Bi-Thio HCP were found to be −15.7 and −13.1 kJ mol^{-1}, respectively. These negative binding energy values led us to conclude that a strong and favorable interaction exists between the iodine and the polymeric network. The interactions between various iodine species are evident from the HOMO and LUMO of the energy-minimized structure of Bi-Thio HCP (Fig. S25). The electrostatic potential (ESP) distribution of Bi-Thio HCP and its iodine-loaded samples (Fig. 5a–c) indicated that the thiophene pendant units produced high local polarization, which promotes electrostatic interactions with the incoming iodine species. The Quantum Theory of Atoms in Molecules (QTAIM) analysis was employed

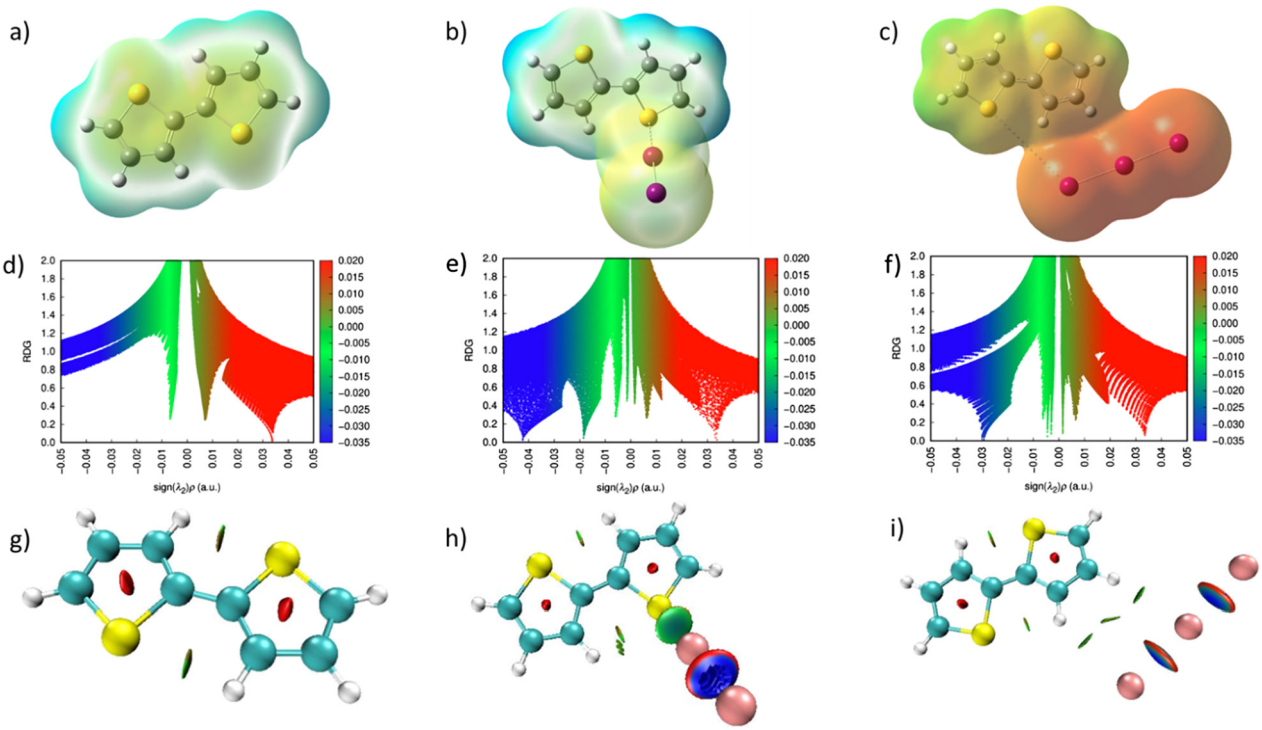

Fig. 5 (a) Electrostatic potential distributions for the structural model of Bi-Thio HCP. (b and c) Electrostatic potential distributions for Bi-Thio HCP after iodine adsorption. (d) RDG analysis of Bi-Thio HCP. (e and f) RDG analysis of Bi-Thio HCP after iodine adsorption. (g) QTAIM topological analysis of Bi-Thio HCP. (h and i) QTAIM topological analysis of Bi-Thio HCP after iodine adsorption.

further to investigate the nature and strength of these interactions. The presence of non-covalent stabilizing interactions is confirmed by the QTAIM plots (Fig. 5g–i), which display unique bond critical points (BCPs) between iodine atoms and the S-functional sites of Bi-Thio HCP. Areas of weak-to-moderate overlap in electron density are highlighted by the blue and green isosurfaces seen in the iodine-loaded Bi-Thio HCP. Additionally, RDG analysis provided a more prominent description of the halogen-bonding interaction. In the comparative RDG analysis of the Bi-Thio HCP and the iodine-loaded Bi-Thio HCP (Fig. 5d–f), spikes appear in the blue and green regions, indicating the presence of iodine nonbonding interactions within the optimized polymeric network. These theoretical results provide strong evidence that the thiophene-rich environment of Bi-Thio HCP is essential for stabilizing iodine species (I_3^-, I_2) *via* orbital polarizations, multi-point noncovalent interactions, and electrostatic attractions.

4. Conclusions

Herein, we describe a facile one-step synthesis of a highly conjugated hyper-cross-linked polymer (HCP) using commercially available yet inexpensive 2,2′-bithiophene as a monomer *via* the well-known Friedel–Crafts alkylation reaction. After a thorough characterization, the hyper-cross-linked polymer (HCP) was investigated as a potential material for iodine adsorption, which occurs in various phases. The iodine uptake capacities of Bi-Thio HCP are superior compared to those of several previously reported porous polymers for similar applications. The adsorbent (Bi-Thio HCP) could be easily regenerated by solvent washing or mild heat treatment. In this process, the Bi-Thio HCP can be recycled without any significant decrease in removal efficiency in further sorption cycles. Using additional experiments and theoretical calculations, the mechanism of interaction between the polymeric network and iodine was studied. Our results suggest that thiophene-functionalized Bi-Thio HCP can be an excellent alternative material for the efficient and selective capture of radioactive iodine vapor during the reprocessing of nuclear fuel. In summary, the porous polymer (Bi-Thio HCP) described here has the potential to be used as an effective adsorbent for environmental remediation applications. We believe our work will enhance the literature on HCP materials, offering improved performance for iodine sequestration.

Conflicts of interest

The authors declare that they have no conflict of interest.

Data availability

The data that support the findings of this study are available in the supplementary information (SI). Supplementary infor-

mation: general characterization and physical measurements, characterization of Bi-Thio HCP, iodine capture data, post capture characterization of Bi-Thio HCP, recyclability experiment data, selectivity experiment data, DFT study, comparison tables. See DOI: https://doi.org/10.1039/d5lp00400d.

Acknowledgements

N. D. acknowledges the Indian Institute of Technology Patna for providing the research facilities. Sk A. W., M. M., and A. H. are thankful to IIT Patna for their respective institute research fellowships. The authors also acknowledge SAIF-IIT Patna for providing access to the TGA and solid-state ^{13}C NMR facilities.

References

1 D. F. Sava, M. A. Rodriguez, K. W. Chapman, P. J. Chupas, J. A. Greathouse, P. S. Crozier and T. M. Nenoff, *J. Am. Chem. Soc.*, 2011, **133**, 12398–12401.
2 A. Davidson, *The role of nuclear energy in the global energy transition*, Oxford Institute for Energy Studies, 2022.
3 N. Tang, J. Liang, C. Niu, H. Wang, Y. Luo, W. Xing, S. Ye, C. Liang, H. Guo and J. Guo, *J. Mater. Chem. A*, 2020, **8**, 7588–7625.
4 R. E. Sims, H.-H. Rogner and K. Gregory, *Energy Policy*, 2003, **31**, 1315–1326.
5 P. Bagla, *Science*, 2015, **350**, 726–727.
6 F. Gralla, D. J. Abson, A. P. Møller, D. J. Lang and H. von Wehrden, *Renewable Sustainable Energy Rev.*, 2017, **70**, 1251–1265.
7 J. Fu, J.-Y. Kang, W. Gao, Z.-W. Huang, L.-Q. Kong, K. Xie, Q.-H. Zhu, G.-H. Zhang, G.-H. Tao and L. He, *Chem. Commun.*, 2025, **61**, 2235–2256.
8 T. J. Robshaw, J. Turner, S. Kearney, B. Walkley, C. A. Sharrad and M. D. Ogden, *SN Appl. Sci.*, 2021, **3**, 843.
9 L. He, L. Chen, X. Dong, S. Zhang, M. Zhang, X. Dai, X. Liu, P. Lin, K. Li and C. Chen, *Chem*, 2021, **7**, 699–714.
10 R. M. Asmussen, J. Turner, S. Chong and B. J. Riley, *Front. Chem.*, 2022, **10**, 1043653.
11 C. Muhire, A. T. Reda, D. Zhang, X. Xu and C. Cui, *Chem. Eng. J.*, 2022, **431**, 133816.
12 F. C. Küpper, M. C. Feiters, B. Olofsson, T. Kaiho, S. Yanagida, M. B. Zimmermann, L. J. Carpenter, G. W. Luther III, Z. Lu and M. Jonsson, *Angew. Chem., Int. Ed.*, 2011, **50**, 11598–11620.
13 S. Abubakar, T. Skorjanc, D. Shetty and A. Trabolsi, *ACS Appl. Mater. Interfaces*, 2021, **13**, 14802–14815.
14 A. Hassan and N. Das, *ACS Appl. Polym. Mater.*, 2023, **5**, 5349–5359.
15 J. E. Ten Hoeve and M. Z. Jacobson, *Energy Environ. Sci.*, 2012, **5**, 8743–8757.
16 J. Li, X. Zhang, M. Fan, Y. Chen, Y. Ma, G. L. Smith, I. J. Vitorica-Yrezabal, D. Lee, S. Xu and M. Schroder, *J. Am. Chem. Soc.*, 2024, **146**, 14048–14057.
17 R. M. Grossi, *Science*, 2021, **372**, 1131.
18 Z. Zheng, Q. Lin, Y. Gao, X. Ji, J. L. Sessler and H. Wang, *Coord. Chem. Rev.*, 2024, **511**, 215860.
19 S. U. Nandanwar, K. Coldsnow, V. Utgikar, P. Sabharwall and D. E. Aston, *Chem. Eng. J.*, 2016, **306**, 369–381.
20 T. Pan, K. Yang, X. Dong and Y. Han, *J. Mater. Chem. A*, 2023, **11**, 5460–5475.
21 Y. Xie, L. Yu, L. Chen, C. Chen, L. Wang, F. Liu, Y. Liao, P. Zhang, T. Chen and Y. Yuan, *Sci. China: Chem.*, 2024, **67**, 3515–3577.
22 W. Xie, D. Cui, S.-R. Zhang, Y.-H. Xu and D.-L. Jiang, *Mater. Horiz.*, 2019, **6**, 1571–1595.
23 Y. Zhang, L. He, T. Pan, J. Xie, F. Wu, X. Dong, X. Wang, L. Chen, S. Gong and W. Liu, *CCS Chem.*, 2023, **5**, 1540–1548.
24 Z. Chen, Q. Lei, Y. Ma, J. Wang, Y. Yan, J. Yin, J. Li, J. Shen, G. Li and T. Pan, *Nat. Commun.*, 2025, **16**, 1169.
25 B. Liu, X. Ren, L. Chen, X. Ma, Q. Chen, Q. Sun, L. Zhang, P. Si and L. Ci, *J. Hazard. Mater.*, 2019, **373**, 705–715.
26 J. Huve, A. Ryzhikov, H. Nouali, V. Lalia, G. Augé and T. J. Daou, *RSC Adv.*, 2018, **8**, 29248–29273.
27 M. Hao, Y. Xie, M. Lei, X. Liu, Z. Chen, H. Yang, G. I. Waterhouse, S. Ma and X. Wang, *J. Am. Chem. Soc.*, 2023, **146**, 1904–1913.
28 D. Shetty, J. Raya, D. S. Han, Z. Asfari, J.-C. Olsen and A. Trabolsi, *Chem. Mater.*, 2017, **29**, 8968–8972.
29 X. Zhang, J. Maddock, T. M. Nenoff, M. A. Denecke, S. Yang and M. Schröder, *Chem. Soc. Rev.*, 2022, **51**, 3243–3262.
30 L. Wang, Z. Li, Q. Wu, Z. Huang, L. Yuan, Z. Chai and W. Shi, *Environ. Sci.:Nano*, 2020, **7**, 724–752.
31 I. Ahmed, Z. Hasan, N. A. Khan and S. H. Jhung, *Appl. Catal., B*, 2013, **129**, 123–129.
32 M. Sharma, P. Sharma, V. C. Janu and R. Gupta, *J. Mater. Chem. A*, 2024, **12**, 26833–26847.
33 J. Wu, F. Xu, S. Li, P. Ma, X. Zhang, Q. Liu, R. Fu and D. Wu, *Adv. Mater.*, 2019, **31**, 1802922.
34 S. Kumar, S. A. Wahed and N. Das, *ACS Appl. Polym. Mater.*, 2025, **7**, 11216–11226.
35 G. Das, T. Skorjanc, S. K. Sharma, F. Gándara, M. Lusi, D. S. Shankar Rao, S. Vimala, S. Krishna Prasad, J. Raya and D. S. Han, *J. Am. Chem. Soc.*, 2017, **139**, 9558–9565.
36 M. S. Lohse and T. Bein, *Adv. Funct. Mater.*, 2018, **28**, 1705553.
37 N. Baig, S. Shetty, S. A. Wahed, A. Hassan, N. Das and B. Alameddine, *ACS Appl. Mater. Interfaces*, 2024, **17**, 17783–17793.
38 P. Bhanja, A. Modak and A. Bhaumik, *ChemCatChem*, 2018, 11.
39 L. Tan and B. Tan, *Chem. Soc. Rev.*, 2017, **46**, 3322–3356.
40 A. Hassan, S. Goswami, A. Alam, R. Bera and N. Das, *Sep. Purif. Technol.*, 2021, **257**, 117923.
41 K. Junthod, B. Todee, K. Khamphaijun, T. Chutimasakul, T. Sangtawesin, T. Ratvijitvech, J. Tantirungrotechai,

U. Suriya and T. Bunchuay, *ACS Appl. Polym. Mater.*, 2024, **6**, 7124–7136.
42 Y. Wang, D. Chen, J. Zhang, C. Wang and X. Li, *Chem. Eng. J.*, 2025, **525**, 170103.
43 C.-J. Sun, P.-F. Wang, H. Wang and B.-H. Han, *Polym. Chem.*, 2016, **7**, 5031–5038.
44 J. Huang and S. R. Turner, *Polym. Rev.*, 2018, **58**, 1–41.
45 H. Ma, J.-J. Chen, L. Tan, J.-H. Bu, Y. Zhu, B. Tan and C. Zhang, *ACS Macro Lett.*, 2016, **5**, 1039–1043.
46 B. Todee, T. Chutimasakul, K. Junthod, A. Docker, P. Saetear, M. Kongkaew, T. Ratvijitvech, J. Tantirungrotechai and T. Bunchuay, *Mater. Chem. Front.*, 2022, **6**, 3023–3032.
47 L. Monnereau, C. Grandclaudon, T. Muller and S. Bräse, *RSC Adv.*, 2015, **5**, 23152–23159.
48 X. Yang and H. Liu, *ACS Appl. Mater. Interfaces*, 2019, **11**, 26474–26482.
49 C. Zhang, Y. He, P. Mu, X. Wang, Q. He, Y. Chen, J. Zeng, F. Wang, Y. Xu and J. X. Jiang, *Adv. Funct. Mater.*, 2018, **28**, 1705432.
50 A. Hassan, A. Kumar, S. A. Wahed, N. Mishra, A. Kumar and N. Das, *Chem. – Eur. J.*, 2025, e01909.
51 A. Hassan, A. Alam, M. Ansari and N. Das, *Chem. Eng. J.*, 2022, **427**, 130950.
52 A. Hassan, A. Alam, S. Chandra and N. Das, *Environ. Sci.: Adv.*, 2022, **1**, 320–330.
53 Z.-Y. Zeng, Z.-C. Lou, L. Hu, W. Dou, X. Zhao, X. Li, J. Fang, X. Qian, H.-B. Yang and L. Xu, *Chem. Eng. J.*, 2024, **496**, 154091.
54 T. Liu, Y. Zhao, M. Song, X. Pang, X. Shi, J. Jia, L. Chi and G. Lu, *J. Am. Chem. Soc.*, 2023, **145**, 2544–2552.
55 S. A. Wahed, A. Hassan, A. Alam, R. Bera and N. Das, *ACS Appl. Mater. Interfaces*, 2025, **7**, 5127–5137.
56 Z. Zheng, Q. Lin, L. Xie, X. Chen, H. Zhou, K. Lin, D. Zhang, X. Chi, J. L. Sessler and H. Wang, *J. Mater. Chem. A*, 2023, **11**, 13399–13408.
57 J. Chang, H. Li, J. Zhao, X. Guan, C. Li, G. Yu, V. Valtchev, Y. Yan, S. Qiu and Q. Fang, *Chem. Sci.*, 2021, **12**, 8452–8457.
58 A. Hassan, R. K. Pandey, A. Chakraborty, S. A. Wahed, T. R. Rao and N. Das, *Soft Matter*, 2024, **20**, 7832–7842.